Article

Journal of
Nanoscience and Nanotechnology
Vol. 15, 8407–8413, 2015
www.aspbs.com/jnn

Fabrication of Sn–3.5Ag Eutectic Alloy Powder by Annealing Sub-Micrometer Sn@Ag Powder Prepared by Citric Acid-Assisted Ag Immersion Plating

Sang-Soo Chee, Eun Byeol Choi, and Jong-Hyun Lee*

Department of Materials Science and Engineering, Seoul National University of Science and Technology, Seoul 139-743, Korea

A Sn–3.5Ag eutectic alloy powder has been developed by chemically synthesizing sub-micrometer Sn@Ag powder at room temperature. This synthesis was achieved by first obtaining a sub-micrometer Sn powder for the core using a modified variant of the polyol method, and then coating this with a uniformly thin and continuous Ag layer through immersion plating in 5.20 mM citric acid. The citric acid was found to play multiple roles in the Ag coating process, acting as a chelating agent, a reducing agent and a stabilizer to ensure coating uniformity; and as such, the amount used has an immense influence on the coating quality of the Ag shells. It was later verified by transmission electron microscopy and X-ray diffraction analysis that the coated Ag layer transfers to the Sn core via diffusion to form an Ag_3Sn phase at room temperature. Differential scanning calorimetry also revealed that the synthesized Sn@Ag powder is nearly transformed into Sn–3.5Ag eutectic alloy powder upon annealing three times at a temperature of up to 250 °C, as evidenced by a single melting peak at 220.5 °C. It was inferred from this that Sn–3.5Ag eutectic alloy powder can be successfully prepared through the synthesis of core Sn powders by a modified polyol method, immersion plating using citric acid, and annealing, in that order.

Keywords: Sn–3.5Ag Nanoparticle, Core–Shell Nanoparticle, Modified Polyol Method, Immersion Plating, Citric Acid, Annealing.

1. INTRODUCTION

Alloys of Sn and Pb have been widely used as solder materials over the past few decades because of their low melting point, superior wettability, and reasonable mechanical properties.[1–4] However, the toxicity of Pb to humans and the environment means that these alloys are now being phased-out in favor of Pb-free alternatives.[2–4] This has led to research into various Pb-free alloys such as Sn–Ag,[5,6] Sn–Cu,[7] Sn–Ag–Cu,[8,9] Sn–Ag–Cu–In,[10] Sn–Zn,[11] and Sn–Bi.[12] Among these, Sn–Ag-based solder containing Sn–3.5 (wt%) Ag and Sn–3.0Ag–0.5Cu have been the ones most readily adopted and used in the electrical and electronic industries.[13,14] Although both have higher melting points (Sn–3.5Ag: 221 °C, Sn–3.0Ag–0.5Cu: 217 °C) and a lower drop reliability than Pb-based solder, they do possess an appropriate solderability and outstanding thermal fatigue reliability.[13] The preparation of Sn–Ag-based alloy powders for use as a filler material in solder pastes has therefore been of significant interest to both academia and industry.

As interconnection technology rapidly evolves and heads toward an ever finer pitch, industry use of solder pastes containing type-7 powders (mostly 2–11 μm in size) has increased, though such usage can be considered to still be at a nascent stage.[15,16] Clearly, the preparation of sub-micrometer Sn–Ag-based solder powders is a research topic that requires immediate attention, yet reports into their preparation seem to be scarce; a fact that can at least partly be attributed to the fact that such sizes are unobtainable with conventional atomization processes.[17] Not surprisingly, there is also a distinct lack of research into printing, soldering, bumping and filling using pastes containing ultrafine solder powders.

The chemical reduction method, consumable-electrode direct current method and supernatant method have all been proposed as suitable approaches to producing sub-micrometer Sn–Ag-based powders.[18–21] Of these, chemical

*Author to whom correspondence should be addressed.

reduction is the more promising, as it offers the advantage of providing control over the size and uniformity of the particles through adjustment of its various process parameters.[22,23] However, this method cannot be easily used for the preparation of alloy powders with a uniform composition due to the different redox potentials of the various metal ions involved under the same reducing atmosphere. That is, the metal ions reduced later through either homogeneous or heterogeneous nucleation have a low probability of homogeneously mixing with other metal ions reduced before them. There is therefore a need for a process that allows greater control over synthesis, thereby ensuring greater compositional uniformity in the alloy powder.

In the present study, one-pot and two-pot syntheses were carried out to produce sub-micrometer, homogenous Sn–3.5Ag alloy powder through a sequence of: preferential formation of sub-micrometer Sn core powder by a modified polyol synthesis process, coating with Ag by immersion plating and finally, forming Ag-coated Sn (Sn@Ag) powder through annealing.

Immersion plating has been used as a convenient method of preparing core–shell powders. For example, Muzikansky et al. reported the preparation of Ag-coated Cu (Cu@Ag) nanoparticles (NPs) at temperatures between 25 and 150 °C by immersion plating without the use of any additives.[24] However, when performed at room-temperature, the use of a general polyol solvent such as diethylene glycol (DEG) makes immersion plating a time-consuming process that is incapable of increasing the coating thickness. Similarly, when performed at a high temperature, it can cause the sub-micrometer metal particles to aggregate and agglomerate. Thus, in order to form a thick and uniform coating of Ag on Sn powder particles at room temperature, a chelating and reducing agent are indispensable. In the present study, citric acid was employed to play multiple roles as both a chelating agent and reducing agent.

2. EXPERIMENTAL DETAILS

Modified polyol and immersion plating methods were adopted to synthesize sub-micrometer Sn@Ag powders, using tin (II) 2-ethylhexanoate [$(CH_3(CH_2)_3CH(C_2H_5)CO_2)_2Sn$, ~95%] and sodium borohydride ($NaBH_4$, 99.99%) as the precursor and reducing agent, respectively. A solvent in the form of DEG (99%), 1,10-phenanthroline monohydrate ($C_{12}H_8N_2 \cdot H_2O$) and a trisodium citrate dihydrate [$HOC(COONa)(CH_2COONa)_2 \cdot 2H_2O$] capping agent were used to prevent oxidation and agglomeration of the Sn powder. To obtain the Ag coating needed for the Sn@Ag powders, silver nitrate ($AgNO_3$, 99.9%, Kojima Chemicals) and citric acid [$HOC(COOH)(CH_2COOH)_2$, 99.5%] were used as the precursor and activating agent, respectively. With the exception of the silver nitrate, all chemicals were supplied by Sigma-Aldrich Co and all were used as-received without any further processing or purification.

2.1. One-Pot Synthesis of Sn@Ag Powders Using Immersion Plating Without Citric Acid

The Sn powder for the core was synthesized at room temperature by injecting tin(II) 2-ethylhexanoate into a solution containing sodium borohydride, 1,10-phenanthroline monohydrate, and trisodium citrate dihydrate. This solution was prepared in advance by dissolving 50 mM of sodium borohydride, 5 mM of 1,10-phenanthroline monohydrate, and 0.34 mM of trisodium citrate dehydrate in 98 mL of DEG and stirring for 3 h. Next, 1 mL of Sn precursor (tin(II) 2-ethylhexanoate) was injected into the DEG solution through a dispenser at a rate of ~4.5 mL/min. To ensure sufficient reaction, the solution was magnetically stirred for 1 h.

The fabrication of the Sn core powder was immediately followed up with Ag coating to synthesize Sn@Ag alloy powder. For this, DEG solution (2 mL) containing 0.912 mM of $AgNO_3$ was added to the solution containing Sn powder at room temperature and magnetically stirred for 2 h. The resulting Sn@Ag powder was washed several times using methanol (99.9%, Duksan Pure Chemical Ltd.) via centrifugation at 4000 rpm for 15 min, and then dried in a vacuum chamber.

2.2. Two-Pot Synthesis of Sn@Ag Powders Using Immersion Plating with Citric Acid

The preparation of the Sn@Ag powder by a two-pot synthesis method, the first stage of which was the Sn core powder method described in the previous section. In the next stage, the DEG solution used to form the Sn powder was first replaced four times with methanol by centrifugation for 15 min at 4000 rpm in order to prevent undesirable reduction of Ag ions by residual BH_4^- ions. The supernatant was then removed to obtain a wet Sn powder that was subsequently added to a DEG solution containing $AgNO_3$ and citric acid. This solution was prepared in advance by adding 0.912 mM of $AgNO_3$ and 2.08–5.20 mM of citric acid to 100 mL DEG. After continuously stirring the mixed solution for 2 h at room temperature using a magnetic bar to ensure a complete coating, the resulting Sn@Ag powder was washed and dried following the same procedure as that used in the one-pot method. This synthesis scheme is presented as Figure 1.

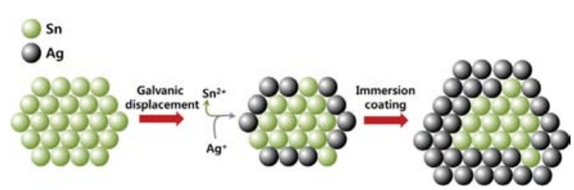

Figure 1. Schematic depicting the preparation of Sn@Ag powder by Ag coating to fabricate a Sn–3.5Ag eutectic alloy powder.

2.3. Characterization

Transmission electron microscopy (TEM, Tecnai G^2 F30ST, FEI Company) was carried out at 300 kV to confirm the morphology, size and crystal structure of the synthesized Sn and Sn@Ag powders. The TEM samples were prepared by placing a few drops of the Sn or Sn@Ag powder solution onto copper grids coated with a carbon film and then drying them. To determine the distribution of elements within the Sn@Ag alloy powder, scanning transmission electron microscopy (STEM) was used under the same conditions as those used for TEM.

X-ray diffraction (XRD, X'pert PRO-MPD, PANalytical) analysis was used to investigate the various crystal phases in the Sn@Ag powders. This analysis was carried out over a 2θ range of 20–90° using Cu-Kα radiation. Thermal analysis was also performed using differential scanning calorimetry (DSC, Q20, TA instruments) to confirm the melting point of the Sn@Ag powder by heating it from 30 to 250 °C at a ramp rate of 10 °C/min. To suppress oxidation of the powder during heating, all experiments were performed under a flow (50 mL/min) of nitrogen gas.

To ascertain the distribution of elements in the Sn@Ag powder annealed at 250 °C for four cycles, electron probe microanalysis (EPMA, JXA-8500F, JEOL) was carried out. The samples for this were prepared by first mounting on epoxy bases, and then finely polishing to reveal the powder in cross-section. A cross-section of the annealed Sn–3.5Ag alloy powder was also closely observed by scanning electron microscopy (SEM, Hitachi S-4300, Hitachi Ltd.), but only after having first etched the sample in a 95 vol.% CH_3OH–4 vol.%HNO_3–1 vol.% HCl solution to enhance the contours of the Ag_3Sn phase.

3. RESULTS AND DISCUSSION

In the modified polyol synthesis method employed, the Sn^{2+} ions dissolved in the DEG solution with 1,10-phenanthroline monohydrate and trisodium citrate dehydrate turned into Sn crystals several tens of nanometers in size in the presence of $NaBH_4$ reducing agent. Upon injecting the solution containing the Ag precursor, continuous Ag shells were gradually formed at an atomic scale on the surfaces of the Sn particles through a galvanic displacement reaction between Sn atoms and Ag^+ ions in solution, as depicted in Figure 1. Given the significant difference in the standard redox potentials of Ag^+/Ag^0 (+0.80 V) and Sn^{2+}/Sn^0 (−0.14 V), this galvanic displacement can be considered spontaneous. However, the coating thickness can only continue to increase for as long as supply and deposition of Ag atoms onto the surface of the Sn particle by the modified polyol reaction is maintained.

In the STEM and elemental mapping images of the Sn@Ag powder synthesized by the one-pot process in Figure 2, Sn quite clearly exists as the main core element. The Ag, however, is not uniformly coated over the surface

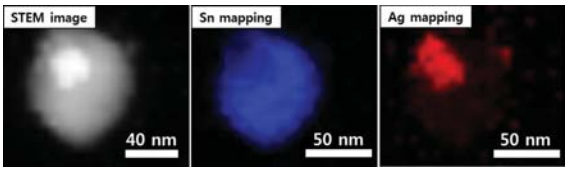

Figure 2. STEM and elemental mapping images of Sn@Ag powder synthesized by a one-pot process.

of the particle, but instead has agglomerated. This non-uniformity can be attributed to the heterogeneous nucleation/growth of Ag ions caused by residual BH_4^- ions in the synthesis of Sn nanoparticles during the later Ag coating reaction. The reduction and coating reactions of the Ag ions involved in the fabrication of the Sn@Ag powder samples in Figure 2 can be represented by the following two reactions for galvanic displacement and reduction by reducing ions:

$$2Ag^+ + Sn^0 \rightarrow Sn^{2+} + 2Ag^0 \quad (1)$$

$$BH_4^- + 8OH^- + 8Ag^+ \rightarrow BO_2^- + 6H_2O + 8Ag \quad (2)$$

In order to synthesize Sn@Ag powder with a uniform Ag coating, galvanic displacement (reaction (1)) needs to be the primary reaction to ensure the slow deposition of Ag atoms. Reaction (2) can, however, occur preferentially if its standard redox potential ($E^0 = 2.04$ V)[25] is substantially higher than that of reaction (1) ($E^0 = 0.94$ V). Moreover, when enhanced by an excess of BH_4^- ions, reaction (2) produces a rapid and localized deposition of Ag, thereby accounting for the fine Ag clusters seen in Figure 2.

Figure 3(a) shows a low-magnification STEM image of a sample synthesized by the one-pot process, revealing not only the Sn@Ag powder, but also a homogenous distribution of fine (<3 nm diameter) Ag NPs. The DSC results of the Sn@Ag powder in Figure 3(b) show that although no melting of the Ag phase occurred upon heating the Sn@Ag powder to 250 °C, it did exhibit two endothermal peaks. The peak at 220.49 °C is indicative of the melting of the eutectic composition (Sn–3.5Ag), while the peak at 230.41 °C indicates the melting of a composition comprised mainly of Sn. The small amount of eutectic composition was obtained through interdiffusion between Sn and Ag atoms upon annealing of the Sn@Ag powder. As can be seen, the intensity of the peak related to pure Sn was much higher than that of the eutectic composition, indicating that the Ag ions did not form a complete shell on the Sn particles, but rather were mostly transformed into free Ag NPs. This agrees well with the results shown in, and inferred, from Figures 2 and 3(a), from which it can be concluded that even with multiple cycles of annealing or long periods at high temperature it would be difficult to completely transform the sample prepared by one-pot synthesis into a homogeneous Sn–3.5Ag eutectic powder.

Wei et al. reported on the immersion plating of Ag onto a silicon wafer sputter-coated with Cu,[26] in which the

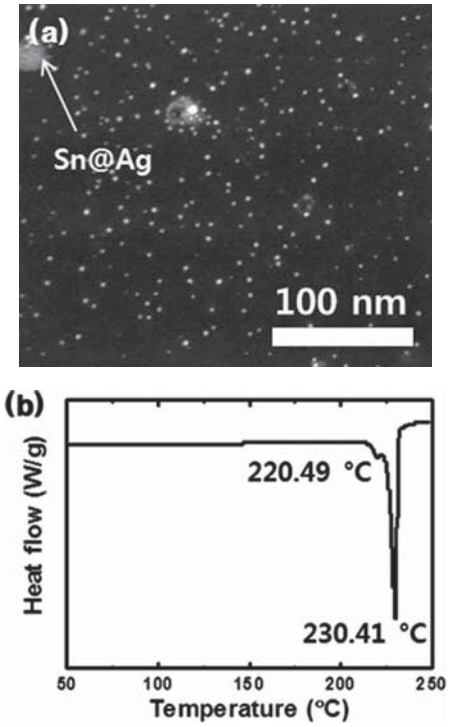

Figure 3. (a) Low-magnification STEM image of a sample synthesized by a one-pot process. Note the formation of free Ag NPs. (b) DSC results of Sn@Ag powder synthesized by the one-pot process.

Ag layer was found to become denser and more uniform with increasing plating time. Citric acid was added to the immersion plating solution in this instance, but no indication was given as to how it influences the plating process. Thus, the two-pot process used in the present study to induce an Ag coating reaction through the repetitive removal of residual ions in the as-synthesized Sn solution was performed with different amounts of citric acid to determine the optimum level to achieve a uniform Ag shell.

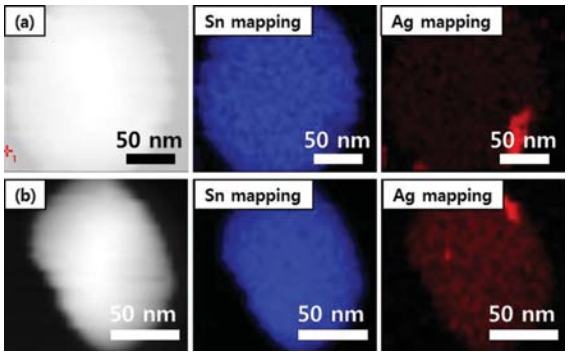

Figure 4. STEM images and element maps of Sn@Ag powder prepared by two-pot synthesis using (a) 4.16 or (b) 5.20 mM of citric acid.

Figure 4(a) shows the distribution of Ag obtained on the surface of a Sn particle using 4.16 mM of citric acid. Though this can be seen to be slightly more uniform than the distribution in Figure 2, uniformity is still clearly quite lacking given that a few Ag clusters can also be observed. Using 5.20 mM of citric acid, on other hand, produced a greatly enhanced uniformity and a clear reduction in the number and size of Ag clusters. Both represent a significant improvement over using no citric acid, however, as this failed to produce any evidence of an Ag coating. Nevertheless, the greater volume and uniformity of the Ag coating produced by using more citric acid implies that citric acid lowers the rate of the immersion coating process by acting as a chelating agent. Indeed, Di et al. have previously reported that citric acid plays a role in controlling nucleation and growth rates as a reducing agent.[27] Thus, it stands to reason that the addition of citric acid would reduce the coating rate through its chelation with Ag ions, with the slower reaction rate in turn being advantageous to ensuring the uniform growth of Ag shells immediately after galvanic displacement. Put simply, in enhancing the uniformity of the Ag coating, citric acid plays multiple roles as a chelating agent, a reducing agent and a stabilizer.

Figure 5 shows TEM images and fast Fourier transform (FFT) patterns of as-synthesized Sn and Sn@Ag powders prepared through immersion coating as a part of the two-pot process. In the FFT patterns of the as-synthesized Sn (inset of Fig. 5(a)), only β-Sn with a plane orientation of (200) was observed, with no oxide phases being detected due to the 1,10-phenanthroline capping agent coating used to suppress oxidation of the particles. After immersion coating (Fig. 5(b)), both β-Sn and Ag_3Sn phases were detected in the FFT patterns, revealing that Ag atoms were adhered to the surfaces of Sn NPs. No pure Ag phase was observed though, and so it is believed that while the thin Ag layer coating was amorphous, Ag_3Sn crystallites were formed through interdiffusion between Sn and Ag at room temperature.

Identification and comparison of the various phases present in the dried Sn@Ag powders synthesized by the one-pot and two-pot processes, was carried out by XRD

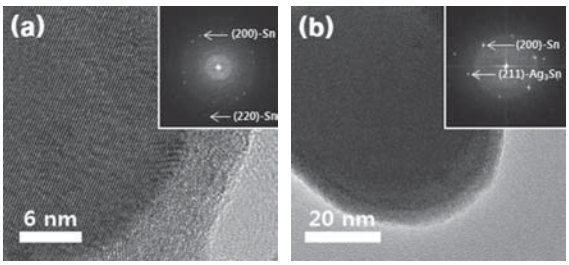

Figure 5. TEM images and FFT patterns (insets) of (a) as-synthesized Sn powder and (b) a Sn@Ag powder prepared by immersion coating in a two-pot process.

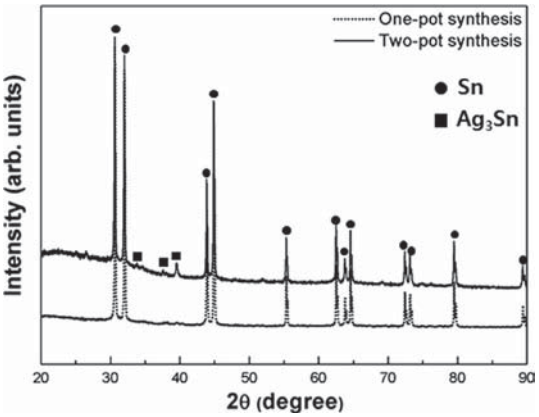

Figure 6. XRD results of Sn@Ag powders synthesized by one-pot and two-pot processes.

measurement. This found that when synthesized by a two-pot process using 5.20 mM of citric acid, both pure Sn and Ag_3Sn phases are formed, as shown in Figure 6. This is consistent with the results in Figure 5(b) and provides further evidence of and effective Ag coating being formed. The intensity of the Ag_3Sn peak was quite weak, but only because XRD does not provide an intense analysis of phases present only on the surface. Meanwhile, only β-Sn phase was detected in the case of the sample synthesized by the one-pot process, as XRD could not detect the small number of fine Ag clusters seen in Figure 2. Neither were there any Ag peaks detected, as any free Ag particles would have been sufficiently removed during the centrifugation stage. In summary, the XRD results clearly show that the two-pot process is superior to the one-pot process when it comes to the effective fabrication of Sn@Ag powders.

To determine how the quality of the Ag coating observed in Figure 4 affects the alloying of Sn with Ag, Sn@Ag powder samples synthesized with the different amounts of citric acid (from 2.08 to 5.20 mM) by the two-pot process were examined using DSC. In the sample synthesized with 2.08 mM of citric acid (Fig. 7(a)), no DSC signal other than that associated with the melting of pure Sn was detected during the first heating cycle. This indicates that an effective Ag coating was only barely formed with such a low concentration of citric acid. Increasing the concentration to 4.16 mM (Fig. 7(b)) produced an obvious melting peak corresponding to the eutectic composition, as well as the peak for pure Sn detected during the first cycle. Interestingly, the intensity of this pure Sn peak decreased during the second heating cycle and saturated from the third heating cycle onwards. This suggests that during the first heating cycle the interdiffusion between Sn and Ag lowers the amount of pure Sn phase forms a greater amount of near-eutetic material, but this mixing of atoms by interdiffusion may be interrupted if there is insufficient Ag coating.

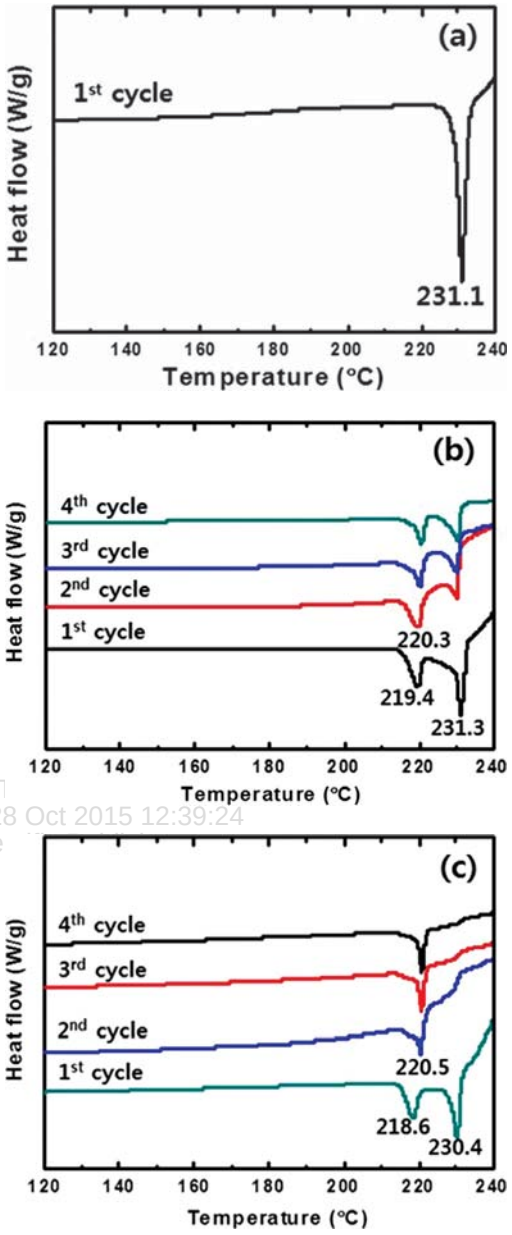

Figure 7. DSC results of Sn@Ag powders prepared by two-pot synthesis with (a) 2.08, (b) 4.16, and (c) 5.20 mM of citric acid.

When 5.2 mM citric acid was used (Fig. 7(c)), the peaks detected had shapes similar to those observed during the first cycle in Figure 7(b). More importantly, the fact that the two peaks of this sample almost merged into one after the second cycle suggests that the amount of Ag that was coated onto the Sn was sufficient. The maximum temperature of this merged peak (220.5 °C) also corresponds well to the melting point of the Sn–3.5Ag eutectic composition, from which it is inferred that the formation of this eutectic was almost fully completed during the earlier heating

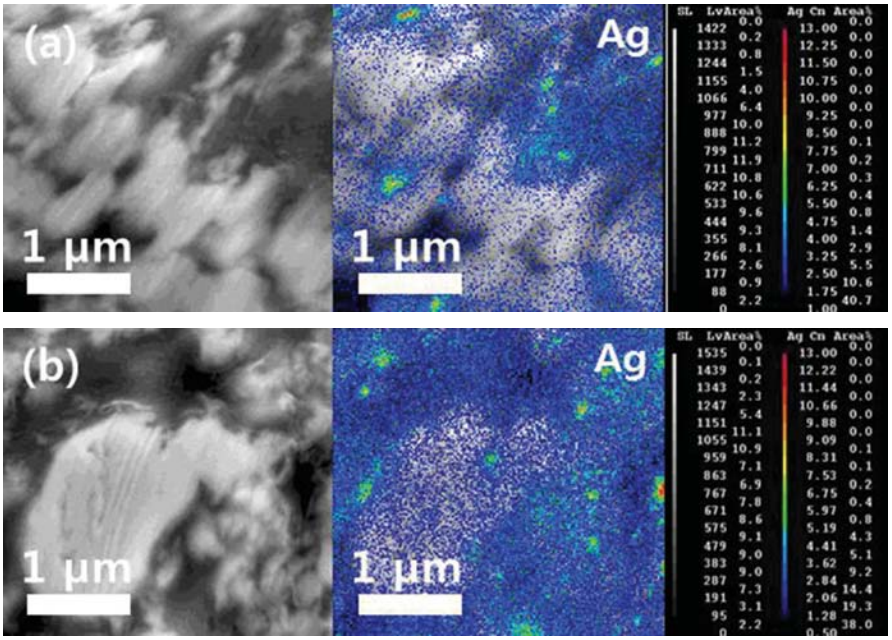

Figure 8. Cross-sectional EPMA images showing the distribution of Ag in Sn–3.5Ag powders prepared by two-pot synthesis: (a) as-synthesized, and (b) after annealing for four cycles at 250 °C.

cycles with this sample. Furthermore, the pure Sn peak almost disappears and the width of the merged peak narrows during the third cycle, indicating the formation of a more perfectly mixed eutectic composition. One interesting observation was the peak at 218.6 °C during the first cycle, which is notably lower than the melting point (221 °C) of the Sn–3.5Ag eutectic. This peak disappeared during the second cycle, forming a unique merged peak at 220.5 °C. This slight decrease in melting point may be the result of the very fine size of eutectic regions, as the Gibbs-Thomson effect is known to reduce the melting of a particle below that of its corresponding bulk form with its size approaches a value of $\leq$30 nm. Thus, the tiny regions of eutectic composition that exist on the surface of the Sn@Ag powder could conceivably melt at a temperature slightly less than that of the equilibrium value.

Figure 8 shows cross-sectional EPMA images of powders synthesized using 5.2 mM citric acid both before and after annealing for four cycles at 250 °C. In the as-synthesized sample shown in Figure 8(a), Ag can be seen to be distributed not only as a shell on the Sn powder, but also in the voids between particles. This suggests that the Ag was located only at the surface of the powder. After annealing (Fig. 8(b)), Ag was clearly observed in the interior of the powder, indicating the diffusion of Ag atoms into the core of the Sn particles. The microstructure of the Sn–3.5Ag alloy powder after annealing was therefore observed further using SEM, which as shown in Figure 9, revealed the presence of a rod-like Ag_3Sn phase.

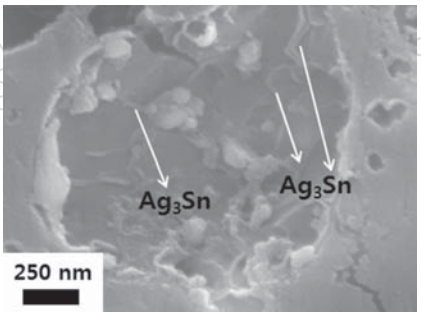

Figure 9. Etched, cross-sectional SEM image of Sn–3.5Ag alloy powder annealed for 4 cycles at 250 °C.

This means that the alloying between Ag and Sn was successfully achieved through annealing.

4. CONCLUSION

Sub-micrometer Sn@Ag powders were successfully fabricated at room temperature using one-pot and two-pot chemical synthesis processes in order to ultimately obtain a Sn–3.5Ag eutectic alloy powder. Synthesis of a sub-micrometer core Sn powder produced only β-Sn with (200) planes; the formation of oxides being inhibited by coating the particles in a 1,10-phenanthroline capping agent. Subsequent one-pot synthesis resulted in Ag clusters being formed on the surface of the Sn particles, with residual BH_4^- ions also producing a great number of free Ag NPs. In contrast, sub-micrometer Sn@Ag powders with

a uniformly thin and continuous Ag layer were obtained through two-pot synthesis using 5.20 mM of citric acid. It was inferred from this that citric acid plays multiple roles as a chelating agent, a reducing agent and a stabilizer. The amount of citric acid added has also been shown to have an immense influence on the quality of the Ag shells. Once formed, the Ag coating layer induces the formation of Ag_3Sn phases via interdiffusion at room temperature. As a result of this, the synthesized Sn@Ag powder is nearly completely transformed into a Sn–3.5Ag eutectic composition upon being subjected to three cycles of annealing at 250 °C, with a characteristic single melting peak at 220.5 °C. This confirms that Sn–3.5Ag eutectic alloy powders can be successfully prepared through a process of two-pot synthesis and subsequent annealing.

Acknowledgment: This study was supported by the Electronics and Telecommunications Research Institute (ETRI). The authors would also like to thank the Korean Basic Science Institute (KBSI) for the TEM, STEM, XRD, DSC, EPMA, and SEM measurements.

References and Notes

1. M. Abtew and G. Selvaduray, *Mat. Sci. Eng. R: Rep.* 27, 95 **(2000)**.
2. S.-H. Wang, T.-S. Chin, C.-F. Yang, S.-W. Chen, and C.-T. Cuang, *J. Alloys Compd.* 497, 428 **(2010)**.
3. C. Zou, Y. Gao, B. Yang, and Q. Zhai, *J. Mater. Sci.: Mater. Electron.* 23, 2 **(2012)**.
4. H. Jiang, K.-S. Moon, F. Hua, and C. P. Wong, *Chem. Mater.* 19, 4482 **(2007)**.
5. W. R. Osório, D. R. Leiva, L. C. Peixoto, L. R. Garcia, and A. Garcia, *J. Alloys Compd.* 562, 194 **(2013)**.
6. Y.-K. Lee, Y.-H. Ko, J.-K. Kim, C.-W. Lee, and S. Yoo, *Electron. Mater. Lett.* 9, 31 **(2013)**.
7. Y. H. Jo, J. C. Park, J. U. Bang, H. Song, and H. M. Lee, *J. Nanosci. Nanotechnol.* 11, 1037 **(2011)**.
8. K.-W. Moon, W. J. Boettinger, U. R. Kattner, F. S. Biancaniello, and C. A. Handwerker, *J. Electron. Mater.* 29, 1122 **(2000)**.
9. S.-S. Chee and J.-H. Lee, *Electron. Mater. Lett.* 10, 637 **(2014)**.
10. J. Sopoušek, M. Palcut, E. Hodúlová, and J. Janovec, *J. Electron. Mater.* 39, 312 **(2010)**.
11. L. R. Garcia, W. R. Osório, L. C. Peixoto, and A. Garcia, *Mater. Charact.* 61, 212 **(2010)**.
12. C. Zhang, S.-D. Liu, G.-T. Qian, and J. Zhou, *Trans. Nonferrous Met. Soc. China* 24, 184 **(2014)**.
13. C. Kanchanomai, Y. Miyashita, Y. Mutoh, and S. L. Mannan, *Mater. Sci. Eng. A* 345, 90 **(2003)**.
14. K. C. Yung, C. M. T. Law, C. P. Lee, B. Cheung, and T. M. Yue, *J. Electron. Mater.* 41, 313 **(2012)**.
15. D. Manessis, R. Patzelt, A. Ostmann, R. Aschenbrenner, and H. Reichl, *Microelectron. Reliab.* 44, 797 **(2004)**.
16. G. J. Jackson, M. W. Hendriksen, R. W. Kay, M. Desmulliez, R. K. Durairaj, and N. N. Ekere, *Solder. Surf. Mount Technol.* 17, 24 **(2005)**.
17. S. Tabatabaei, A. Kumar, H. Ardebili, P. J. Loos, and P. M. Ajayan, *Microelectron. Reliab.* 52, 2685 **(2012)**.
18. Y. Gao, C. Zou, B. Yang, Q. Zhai, J. Liu, E. Zhuravlev, and C. Schick, *J. Alloys Compd.* 484, 777 **(2009)**.
19. C. D. Zou, Y. L. Gao, B. Yang, X. Z. Xia, Q. J. Zhai, C. Andersson, and J. Liu, *J. Electron. Mater.* 38, 351 **(2009)**.
20. C. Y. Lin, J. H. Chou, Y. G. Lee, and U. S. Mohanty, *J. Alloys. Compd.* 470, 328 **(2009)**.
21. C. Zou, Y. Gao, B. Yang, and Q. Zhai, *J. Mater. Sci.: Mater. Electron.* 21, 868 **(2010)**.
22. L.-Y. Hsiao and J.-G. Duh, *J. Electrochem. Soc.* 152, J105 **(2005)**.
23. J. Chen, G. Wang, X. Wang, J. Tian, S. Zhu, and R. Wang, *J. Nanosci. Nanotechnol.* 13, 7008 **(2013)**.
24. A. Muzikansky, P. Nanikashvili, J. Grinblat, and D. Zitoun, *J. Phys. Chem. C* 117, 3093 **(2013)**.
25. S. C. Amendola, P. Onnerud, M. T. Kelly, P. J. Peillo, S. L. Shar-Goldman, and M. Binder, *J. Power Sources* 84, 130 **(1999)**.
26. Z. Wei, D. Tang, and T. O'Keefe, *China Particuol.* 3, 271 **(2005)**.
27. W. Di, M.-G. Willnger, R. A. S. Ferreira, X. Ren, S. Lu, and N. Pinna, *J. Phys. Chem. C* 112, 18815 **(2008)**.

Received: 15 November 2014. Accepted: 27 January 2015.